Made available by Hasselt University Library in https://documentserver.uhasselt.be

Dispersity and Architecture Driven Self-assembly and Confined Crystallization of Symmetric Branched Block Copolymers

Peer-reviewed author version

PITET, Louis; Chamberlain, Bradley; Hauser, Adam & Hillmyer, Marc (2019)
Dispersity and Architecture Driven Self-assembly and Confined Crystallization of Symmetric Branched Block Copolymers. In: Polymer Chemistry, 10 (39), p. 5385-5395.

DOI: 10.1039/C9PY01173K
Handle: http://hdl.handle.net/1942/29807

Dispersity and Architecture Driven Self-assembly and Confined Crystallization of Symmetric Branched Block Copolymers

Louis M. Pitet[†§]*, Bradley M. Chamberlain[‡], Adam W. Hauser[†] and Marc A. Hillmyer[†]*

[†]*Department of Chemistry, University of Minnesota, 207 Pleasant St. SE, Minneapolis, Minnesota 55455-0431, United States,* [§]*Institute for Materials Research (IMO) and Department of Chemistry, Hasselt University, Martelarenlaan 42, 3500 Hasselt, Belgium*

[‡]*Department of Chemistry, Luther College, 700 College Drive, Decorah, Iowa 52101, United States*

* To whom correspondence should be addressed (e-mail: louis.pitet@uhasselt.be; hillmyer@umn.edu)

Abstract

The effect of macromolecular architecture on the morphology and thermal characteristics of triblock copolymers was evaluated for linear, H-shaped, and arachnearm architectures with poly(*cis*-cyclooctene) (PCOE) midblocks flanked with arms of poly(d,l-lactide) (PLA). Chain topology was found to significantly influence the interfacial curvature of the microphase separated domains, as implicated by morphological differences observed by transmission electron microscopy (TEM) and small-angle x-ray scattering (SAXS). The branched molecular architectures and molar mass dispersities (*Đ*) of the triblock polymers examined here resulted in a significant shift in the phase boundaries between conventional equilibrium microphase separated structures to higher volume fractions of the end blocks (i.e., PLA) as compared to conventional low dispersity linear triblocks. Macromolecular topology was also found to strongly influence the extent of homo- vs. heterogeneous nucleation in the semi-crystalline PCOE block. The culmination of the bulk phase behavior analysis demonstrates the ability to fine-tune the properties of the block polymers by exploiting different architectures through a synthetically straightforward route.

INTRODUCTION

Macromolecular self-assembly is a powerful tool to tune the design of complex patterns at the nanoscale using bottom-up design principles. Towards this end, block polymers are fascinating hybrid macromolecules comprised of two or more segments of different repeating units connected covalently. Strong enthalpic repulsions between dissimilar blocks drive block polymers to segregate at the nanoscale, and the symmetry and periodicity of the resulting self-assembled morphologies can be precisely tuned through the molar mass (N), composition (f), architecture (linear vs. branched vs. graft), and dispersity, among other factors. Adding more blocks (e.g., as in ABC triblock terpolymers) or altering the connectivity (ABAB… multiblock copolymers) naturally increases the architectural complexity and provides a way to fine-tune the properties and nanoscale patterns typically associated with these systems.[1-3] As a result, synthetic pathways toward branched block copolymers have garnered a great deal of attention as an additional route towards complex self-assembled morphologies.[4-12] Here we explore well-defined symmetric branched block polymers comprising poly(*cis*-cyclooctene) (PCOE) midblocks and poly(d,l-lactide) (PLA) end-blocks. The architecture is systematically varied to access linear, H-shaped, and arachnearm architectures. Furthermore, the end and midblocks have disparate molar mass dispersities ($Đ$) owing to the different mechanisms of polymerization (Scheme 1). Detailed synthetic descriptions of such block polymers have been previously reported.[13]

Scheme 1. Synthesis of linear, H-shaped, and arachnearm L_xCL_x symmetric block copolymers

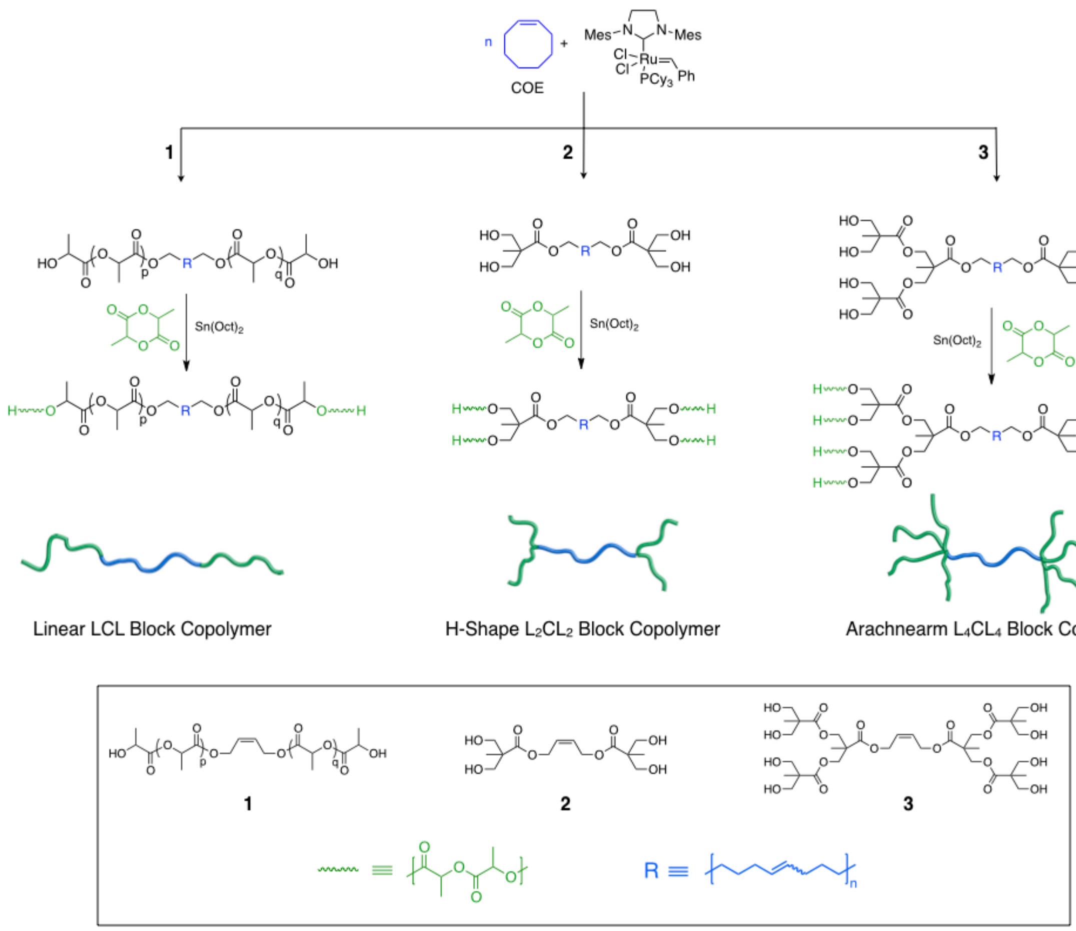

The influence of branching on the interfacial curvature between the mesoscale phase-separated domains has been explored theoretically (Figure S1a).[14-17] There are several reports describing the synthesis of relatively narrow dispersity block copolymers with simple graft (i.e., A_2B) [18-25] and H-shaped (i.e., A_2BA_2)[26-34] architectures. The general consequence of branching manifests itself as increased interfacial curvature away from the component with the greater number of chains converging at the block junctions (i.e., the green PLA component in Scheme 1). This has significant ramifications on the morphology maps for these systems, as the composition and arm-asymmetry combined with conformational asymmetry associated with disparate statistical segment lengths can noticeably shift the microphase boundaries relative to linear and conformationally symmetric counterparts.[33] The effect of macromolecular topology on the observed phase behavior can be expressed by the asymmetry parameter (ε, eq 1).[15]

$$\epsilon = \left(\frac{n_A}{n_B}\right)\left(\frac{\beta_B^2}{\beta_A^2}\right)^{0.5} \tag{1}$$

where n_i is the number of arms of repeating unit "i" emanating from a block juncture and $\beta_i^2 = R_g^2/V = a_i^2/(6v_i)$, [$a$ = statistical segment length; v_i = standard segmental volume; R_g = radius of gyration]. The latter essentially indicates the relative flexibility of a particular component (see Supporting Information, page S9 for a detailed analysis of the statistical parameters associated with PLA and PCOE).[35] A conformationally symmetric block copolymer with an A_2B architecture has a value of $\varepsilon = 2.0$. As an example of the consequences of architecture on morphology, a linear ABA triblock copolymer with 45 vol % midblock (PCOE here) would be predicted to adopt a lamellar morphology based on self-consistent field theory (SCFT) for $Đ$ = 1.0. However, an analogous branched block polymer with the same composition (45 vol % B-block) but with an A_2B architecture would be expected to adopt cylinders of the B-block, due to an increase in interfacial curvature resulting from contributions of the branched topology to the conformational asymmetry of the graft block polymer.[36]

In addition to the macromolecular topology, molar mass dispersity also affects the phase boundaries in block polymers. The contrasting $Đ$ for the two constituent blocks in ABA triblocks (i.e. $Đ_A \approx 1$ and $Đ_B \approx 2$) typically shifts the morphology map toward higher volume fractions of the midblock compared to the low-dispersity counterparts (Figure S1c).[37-40] For example, the hypothetical linear triblock polymer with 45 vol % midblock that was discussed in the previous paragraph would be expected to adopt a cylindrical morphology rather than a lamellar morphology after accounting for midblock molar mass dispersity. Thus, both of these features (i.e., dispersity and branching) drive the interfacial curvature towards the more disperse PCOE block and away from the branched PLA block, shifting the phase boundaries toward higher volume fraction of midblock (PCOE). The interaction parameter of the PCOE-*b*-PLA system was not reported previously, though the anticipated value is high based on other polyolefin–PLA block copolymers.[41-47]

This report evaluates crystallization and bulk phase behavior for symmetric triblock copolymers with varying molecular architectures of the type A_xBA_x, for which x = 1, 2, or 4.[13] The midblock component was synthesized by ring-opening metathesis polymerization (ROMP) of *cis*-cyclooctene (COE) with a chain-transfer agent to prepare hydroxy-telechelic PCOE. Several different CTAs were used to impart different multiples of hydroxyl functionality to initiate subsequent ring-opening transesterification polymerization (ROTEP) of d,l-lactide and achieve the desired branched block copolymers with linear (x = 1), H-shaped (x = 2), and arachnearm (x = 4) architectures (Scheme 1). The cross-metathesis (i.e., chain-transfer) utilized in the first polymerization gives polymers with molar mass distributions approaching 2. Comparatively, ROTEP provides blocks with low dispersity ($Đ < 1.2$). Both the large molar mass dispersity and the branched architectures can lead to significant deviation from the traditional bulk phase behavior associated with conventional linear block copolymers having near monodisperse size distributions.[14, 15, 17, 36, 48-56]

RESULTS AND DISCUSSION

Morphological Characterization of Selected Block Copolymers

A series of block copolymers with different architectures was prepared as described previously.[13] Bulk self-assembly is presented for a select number of samples (Table 1) to exemplify the influence of molecular architecture, whereas crystallization analysis by differential scanning calorimetry (DSC) was performed on all the block copolymers (Table S1).[i] Sample identifiers are of the general form L_xCL_x [$\#_x$–#–$\#_x$], where *x* refers to the number of arms emanating from the block junction (i.e., *x* = 2 → H-shaped) and # refers to the approximate molar mass of the respective segments in kg mol^{-1}.

---

[i] All block copolymers were evaluated with the exception of the H-shaped block copolymer having composition with approximately 15 wt % PLA.

Table 1. Molecular characteristics of several block copolymers prepared for morphological analysis.

Sample ID	$M_{n,total}$[a]	$M_{n,PLA}$[b]	w_{PLA}[c]	f_{PLA}[d]	$Đ_{PCOE}$[e]	$Đ_{total}$[e]	morphology[f]	d^*[g]
	kg mol^{-1}	kg mol^{-1}						nm
L_4CL_4 [0.4_4-27-0.4_4]	29.9	3.0	0.12	0.09	1.81	1.80	lamellar	26.0
L_2CL_2 [2_2-23-2_2]	29.5	7.0	0.26	0.19	1.71	1.57	lamellar	32.2
LCL [10-22-10]	41.1	18.6	0.46	0.38	1.70	1.37	lamellar	35.7
L_2CL_2 [5_2-23-5_2]	40.8	18.0	0.46	0.37	1.71	1.38	cylinders (disorganized)	35.5
LCL [21-22-21]	64.1	41.6	0.66	0.57	1.70	1.27	lamellar	38.5
L_2CL_2 [10_2-23-10_2]	64.5	41.6	0.66	0.57	1.71	1.23	cylinders	30.2

[a] Calculated from the M_n (from NMR) of the precursor/macroinitiator PCOE as a reference, combined with the relative intensities of the respective repeat unit signals obtained from ^{1}H NMR spectroscopy. [b] Reported as the total molecular weight of PLA obtained from ^{1}H NMR spectroscopy; the molar mass per PLA block can be obtained by dividing by 2 for the linear copolymers or dividing by 4 for the H-shaped copolymers. [c] Calculated from the relative intensities of the repeat unit signals in ^{1}H NMR spectroscopy and using the respective repeating unit molar mass. [d] Calculated based on the weight fractions and the densities of the respective components at ambient temperature: $\rho_L = 1.25$ g mL^{-1} (ref. [57]) and $\rho_C = 0.89$ g mL^{-1} (ref. [58]) [e] Determined from SEC measurements compared with polystyrene standards. [f] Determined from the relative position of reflections in SAXS profiles in relation to the principal scattering vector. [g] Calculated based on the position of the principal scattering vector (q^*) and the relationship $d^*=2\pi/q^*$.

SAXS measurements at 160 °C are shown for three samples having different architectures and different compositions, yet all exhibiting profiles consistent with lamellar morphologies (Figure 1). The linear LCL [21-22-21] has a volume fraction of PLA equal to approximately f_L

= 0.57 (f_C = 0.43) and exhibits a pattern that is characteristic of a lamellar sample with average domain periodicity ($d^* = 2\pi/q^*$) of 37 nm (Figure 1a). This is well within the calculated lamellar phase window predicted for a symmetric, linear ABA-type triblock copolymer.

In other related work, linear ABA-type triblock copolymers with high-$Đ$ midblocks were shown to adopt lamellae between f_B = 0.25 – 0.48, representing a substantial shift of the phase boundaries toward higher volume fraction of disperse midblock.[39] This is similar to the system described here having a rather high-$Đ$ midblock of PCOE ($Đ$ = 1.7) and relatively low-$Đ$ PLA arms. The lamellar morphology is therefore in line with the observations of others and also with more recent calculations interrogating the effect of block dispersity on phase behavior.[49]

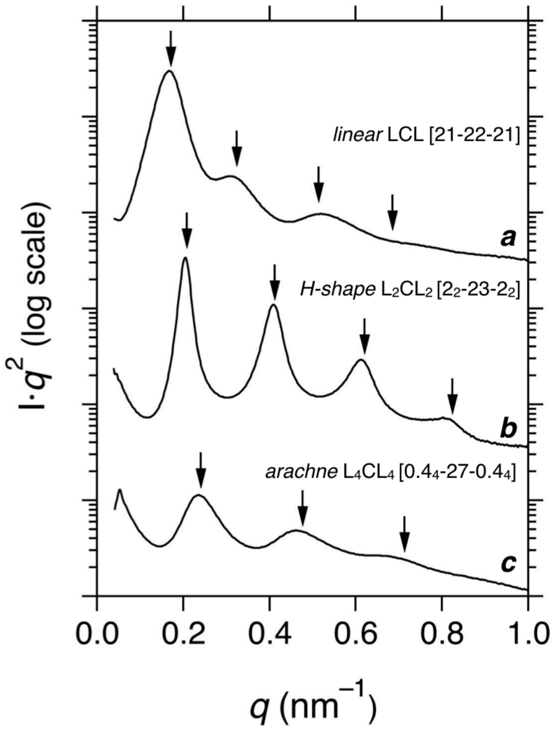

Figure 1. One-dimensional SAXS profile at 160 °C for (a) the linear block copolymer LCL [21–22–21] having f_L = 0.57; (b) the H-shaped block copolymer L$_2$CL$_2$ [2$_2$-23-2$_2$] having f_L = 0.19 and (c) the arachnearm block copolymer L$_4$CL$_4$ [0.4$_4$-27-0.4$_4$] having f_L = 0.09 . Arrows indicate the predicted positions of Bragg reflections based on the structure factor for a lamellar morphology related to the position of the primary scattering peak at q^*.

The L$_2$CL$_2$ [2$_2$–23–2$_2$] sample (Table 1) with a volume fraction of PLA (f_L) ≈ 0.19 also adopted a lamellar morphology as corroborated by TEM (Figure 2) and SAXS analyses (Figure 1b). The average lamellar spacing is approximately 30 nm as measured by TEM micrographs and is generally consistent with the principal spacing as measured by SAXS (d^* = 32 nm). The average ratio of thickness between the light PLA and dark PCOE layers is approximately 1:4, consistent with the estimated volume fraction of PLA. The observation of a lamellar morphology at such a high volumetric asymmetry was surprising as f_L lies well outside of the typical range where lamellar morphologies are expected in linear ABA triblocks with either low or high $Đ$ ($Đ_A$ = 1.0; $Đ_B$ = 1.5) (see Figure S1).[37, 49-51, 59] On the basis of theoretical predictions for the individual parameters (*i.e.*, statistical segment length and dispersities, Eq 1) associated with this system, the branching is likely the largest contributor for the lamellar phase at such high compositional asymmetry.[15] Similarly, lamellar morphologies were observed for linear-dendritic block copolymers having asymmetric compositions that lie outside of the predicted lamellar phase window for linear counterparts. For example linear polystyrene combined with a dendritic poly(benzyl ether) block adopted a lamellar morphology with w_{PS} equal to 0.69[60] while linear polystyrene combined with dendritic poly(propylene imine) adopted a lamellar morphology when w_{PS} = 0.75.[61]

Finally, the SAXS profile captured at 160 °C for the arachnearm copolymer L_4CL_4 [0.4_4-27-0.4_4] also exhibits a pattern that suggests a lamellar morphology with a domain spacing of d^* = 26 nm. This is the smallest of the periodicities seen for these three samples, despite not having the lowest molar mass. This is further indicative of the impact that branching has on the interfacial geometry. This composition lies far outside the expected phase window for a linear copolymer with high dispersity. While a TEM image was not captured for this sample, morphological assignment is in agreement with the expected morphology for a conformationally symmetric A_4B copolymer based on SCFT (Figure S1).[14]

The comparison of scattering patterns exhibited by the samples from the three different architectures (linear, H-shaped, arachnearm) suggests that long-range ordering decreases with increasing branching. This is consistent with the observations described for other branched block polymers.[62] This trend may also have contributed with the increased difficulty of capturing TEM micrographs associated with the arachnearm architectures. Likewise, the

SAXS scattering reflections are routinely broader for branched samples than for linear samples throughout this study

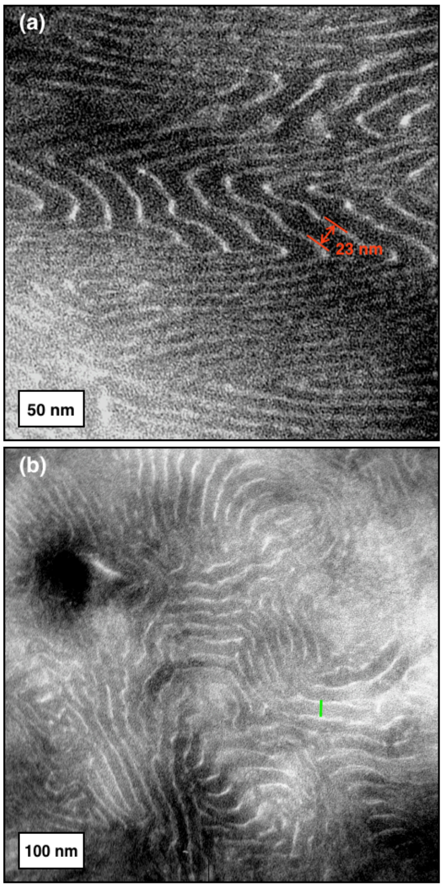

Figure 2. TEM micrographs for sample L_2CL_2 [2_2–23–2_2] collected at magnifications of (a) ×50,000 and (b) ×25,000. PCOE is stained dark with OsO_4 vapor in the TEM micrographs.

One-dimensional SAXS profiles were collected for L_2CL_2 [2_2–23–2_2] at increasing temperatures during heating in the melt after annealing for approximately 5 minutes at each temperature (Figure 3). Subsequent measurements were then collected upon cooling and annealing at 40 °C and finally at 25 °C. The data are consistent with a lamellar morphology at all temperatures above melting of PCOE ($T_{m,C}$ = 50 °C) as indicated by several higher order scattering reflections with strong intensity and maxima occurring at integral multiples of the principal scattering vector q^*. At ambient temperature, the PCOE segment has presumably crystallized, which is responsible for the attenuation of higher order reflections. However, the position and breadth of the principle scattering vector suggests that the morphology has been retained during crystallization (vide infra). The retention of the morphology and the strong scattering contrast observed in these samples likely arises from the anticipated strong immiscibility between PLA and hydrocarbon-based polymers, as previously detailed for systems having similar chemical structures.[63]

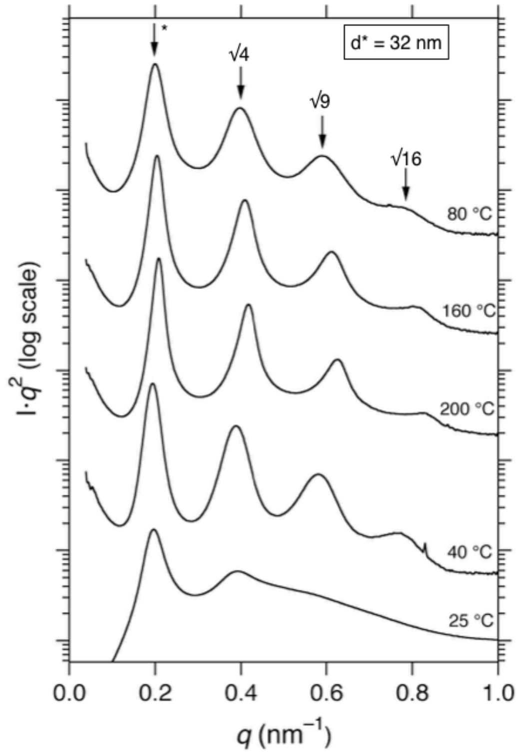

Figure 3. One-dimensional SAXS profiles For H-shaped block copolymer L_2CL_2 [2_2–23–2_2] collected at various temperatures in the melt (T = 80, 160, 200, 40 °C > $T_{c,C}$) and crystalline (T = 25 °C < $T_{m,C}$) states. The top SAXS profile (80 °C) has arrows indicating the position of the primary scattering peak (q^*) and corresponding predictions for higher order peak positions associated with Bragg reflections for a lamellar morphology ($\sqrt{4}q^*$, $\sqrt{9}q^*$, $\sqrt{16}q^*$).

To more directly examine the effect that macromolecular architecture has on the resulting self-assembled morphology, a linear LCL triblock (LCL [10–22–10]) was compared to its H-shaped analog (L_2CL_2 [5_2–23–5_2]) with a nearly identical f_{PLA} yet different chain topology. Analysis of the linear LCL [10–22–10] (f_L = 0.38) by SAXS reveals a profile consistent also with a lamellar morphology with d^* = 35.8 nm (Figure 4). The value of f_L equal to 0.38 falls within the lamellar window predicted theoretically for an AB diblock copolymer with disparate $Đ$ (Figure S1). In contrast, the H-shaped analog of this copolymer, L_2CL_2 [5_2–23–5_2], displayed a morphology consistent with disorganized dispersion of cylindrical-like domains, with d^* = 35.5 nm based on SAXS and TEM analyses (Figure 5), despite having a nearly identical molar mass and composition as LCL [10-23-10]. Again, this confirms that chain architecture is an important determining factor in the self-assembled morphologies for these triblocks.

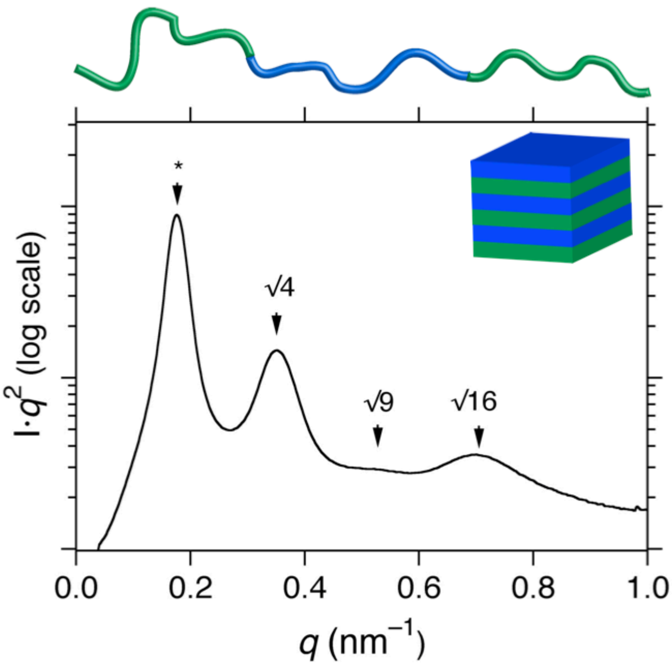

Figure 4. One-dimensional SAXS profile at 25 °C for the linear block copolymer LCL [10–22–10] having w_L = 0.46 and f_L = 0.38 at ambient temperature as calculated using densities of the respective homopolymers. Arrows indicate the predicted positions of Bragg reflections based on the structure factor for a lamellar morphology related to the position of the primary scattering peak at q^* = 0.177 nm^{-1}.

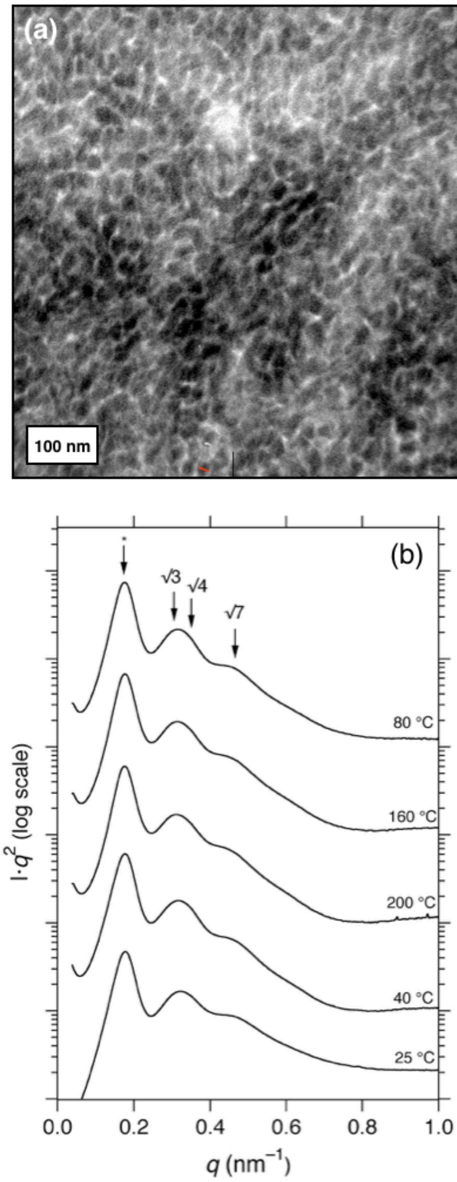

Figure 5. L$_2$CL$_2$ [5$_2$–23–5$_2$] block copolymer: (a) TEM micrograph showing the darkly stained (with OsO$_4$) PCOE domains on the concave side of the domain interfaces and (b) one-dimensional SAXS profiles at various temperatures with arrows indicating the predicted positions of Bragg reflections associated with a hexagonally packed cylindrical lattice.

A more detailed TEM analysis of the microphase separated domains of L$_2$CL$_2$ [5$_2$–23–5$_2$] revealed an array of microdomains with poor long-range spatial correlations, with the stained PCOE domains situated on the concave side of curved interfaces. This image is not unlike the morphologies identified by Mahanthappa and coworkers for similarly polydisperse symmetric triblock copolymers of poly(styrene)-*b*-poly(butadiene)-*b*-poly(styrene).[64] The authors described several triblock copolymers with nearly symmetric compositions and observed molar mass independent adoption of a disordered, bicontinuous morphology. Sample L_2CL_2 [5_2–23–5_2] has larger compositional asymmetry than the symmetric counterparts reported by Mahanthappa, with PCOE constituting the majority component by volume. However, based on the TEM micrographs, PLA nevertheless resides predominantly on the convex side of the curved interfaces, suggesting that it occupies the matrix domain. However, a disorganized structure with both components forming continuous paths cannot be ruled out. Linear samples with comparable molar mass and composition to L_2CL_2 [5_2–23–5_2] have been observed to adopt bicontinuous, poorly organized structures in similar systems.[38]

Unambiguous assignment of an ordered morphology is difficult based on SAXS analysis of L_2CL_2 [5_2–23–5_2] (Figure 5b). The patterns suggest distinct microphase separation above the melting temperature (80, 160, 200 °C > $T_{m,C}$) and are consistent with retention of the morphology after cooling below $T_{c,C}$. The primary scattering peak is positioned at $q^* = 0.177$ nm^{-1} at 80 °C ($d = 35.8$ nm). This domain size is nearly identical to the linear analog LCL [10–22–10]. However, the shape and position of higher order reflections for the H-shaped L_2CL_2 [5_2–23–5_2] are unique compared with its linear analog. Most notably, a broad reflection centered near $q^*\sqrt{7} = 0.47$ nm^{-1} is suggestive of a cylindrical morphology. Additionally, the wide breadth of the secondary scattering reflection covers the region in which two other characteristic signals for hexagonally packed cylinders would be anticipated, namely $q^*\sqrt{3}$ and $q^*\sqrt{4}$ (see arrows in Figure 4b). Collectively, these features suggest a hexagonal symmetry, though lacking long-range organization and perhaps mixed with a disordered microphase separated structure as observed by TEM. For the benefit of comparison, we calculated the average cylinder radius (r_c) assuming a well-ordered hexagonal array and the interplanar domain spacing obtained by SAXS with $f_C = 0.63$ at 25 °C, which gave a value $r_c = 12.1$ nm. On the basis of the TEM micrograph in Figure 5a, the average radius of the circular domains ranges from 9–13 nm, which is reasonably consistent with the SAXS analysis.

Brief analysis of two additional samples differing only in molecular architecture helps to emphasize the influence that chain topology has on morphology. Namely, linear LCL [21–22–21] and H-shaped L_2CL_2 [10_2–23–10_2] both have $w_L = 0.66$ ($f_L = 0.57$ at 25 °C). SAXS patterns of the linear block copolymer at various temperatures from 25–200 °C are consistent with a lamellar morphology with *d*-spacing of 38.5 nm ($q^* = 0.163$ nm^{-1}) (Figure 6a). Crystallization is presumably confined within the lamellar microdomains established in the melt as evinced by the similitude of profiles taken above and below $T_{c,C}$ (*vide infra*).[65] This behavior is consistent with the high T_g of the non-crystallizing PLA block as well as with the expected large interaction parameter between PLA and PCOE. The lamellar morphology in the linear triblock falls within a composition range predicted for compositionally symmetric monodisperse triblock copolymers and polydisperse diblock copolymers. Theoretical treatment of polydisperse triblock copolymers also illustrates that nearly symmetric composition is predicted to adopt a morphology with flat interfaces.[49]

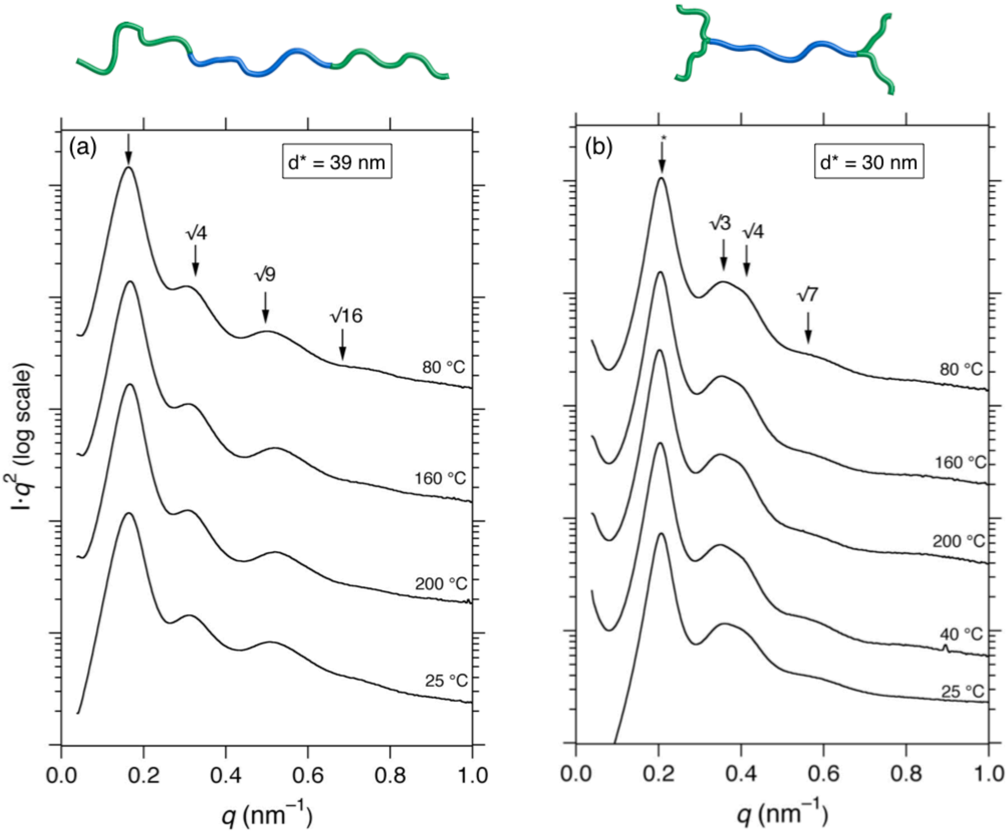

Figure 6. One dimensional SAXS profiles at various temperatures for (a) linear triblock copolymer LCL [21–22–21] with $w_L = 0.66$ and $f_L = 0.57$ (at 25 °C) exhibiting higher order reflections consistent with a lamellar morphology and (b) H-shaped block copolymer L_2CL_2 [10_2–23–10_2] with $w_L = 0.66$ and $f_L = 0.57$ (at 25 °C) exhibiting higher order reflections consistent with a cylindrical morphology. Morphology assignments are based on the correlation of reflection positions with the predicted positions of Bragg reflections consistent with the lattice parameters.

The H-shaped L_2CL_2 [10_2–23–10_2] exhibits scattering profiles consistent with a hexagonal array of cylinders, despite having a nearly identical composition to the lamellar-forming linear triblock (Figure 6b). There appear clearly demarcated, albeit relatively broad, reflections occurring at multiples of √3, √4, and √7 to the principle scattering peak at $q^* = 0.208\ \text{nm}^{-1}$ at 80 °C (above $T_{\text{c, C}}$). The small shift in peak position with changing temperature is consistent with the expected dependence of q^* with temperature. Cylinder radius r_c was approximated to be 8.5 nm based on the value $f_C = 0.43$ at 25 °C and the corresponding domain spacing of $d^* = 30.2$ nm.

Comparing the domain spacing obtained from SAXS between the two samples in Figure 6 (copolymers L_2CL_2 [10_2–23–10_2] and LCL [21–22–21]) suggests that two different morphologies are adopted. Mean-field approximations predict that a sample exhibiting hexagonally packed cylinders will have a smaller principle domain spacing than a sample with identical molecular weight that adopts a lamellar morphology.[66] A summary of the morphological features in the selected block copolymers described above is provided in Table 1.

Crystallization of Branched Block Copolymers

Lastly, the bulk morphologies of block copolymers containing at least one semicrystalline component typically exhibit strong path dependence.[67] The behavior is closely tied to the relative values of T_g of the amorphous component and the T_m of the semicrystallline component. Amorphous PLA exhibits $T_{g,L}$ of approximately 45 °C ± 5 °C and PCOE is semi-crystalline with $T_{m,C}$ of approximately 55 °C ± 5 °C and crystallization temperature ($T_{c,C}$) of approximately 35 °C at standard heating/cooling rates of 10 °C min^{-1}.

PLA and PCOE block polymers in this study are all expected to occupy the strong segregation regime due to their large estimated interaction parameter, χ.[39] Combining strong segregation with the relationship between the relevant transition temperatures ($T_{g,L} > T_{c,C}$) suggests that crystallization occurs within the confined domains of the microphase separated structures established in the melt.[68, 69] That is, annealing at elevated temperatures ($T >> T_{m,C}$) followed by cooling at a moderate rate (~10–50 °C min^{-1}) should result first in PLA vitrification followed by crystallization of PCOE within the confines templated by the glassy PLA.

Indeed, measurement of the SAXS profile of at 25 °C (bottom profile in Figure 3) shows minimal difference in the intensity and breadth of the primary scattering peak, suggesting that the morphology is preserved upon crystallization. The higher order reflections are less pronounced at ambient temperature than at $T > T_{c,C}$ (where $T_{c,C}$ is the crystallization temperature of PCOE – vide infra) and are dominated by a broad reflection. The broad halo surrounding the intense scattering peak suggests substantial crystallinity, which is consistent with the DSC results ($T_{c,C} \approx 35$ °C). The consistent q^* of the scattering reflections suggest that crystallization is confined within the microdomains established in the melt. Crystal confinement is expected on the basis of the relative thermal transitions of the amorphous PLA, which first vitrified and thereby anchored the PCOE chain ends and constrained crystallization within the pre-formed microdomains.[67, 70] This retention of microphase separation during the crystallization is amplified by the strong segregation strength anticipated for this system. Indeed, wide-angle x-ray scattering (WAXS) profiles collected at 25 °C show two reflections that are characteristic of a triclinic structure having lattice dimensions of 4.5 and 3.9 Å associated with semi-crystalline PCOE (Figure 7).[71, 72]

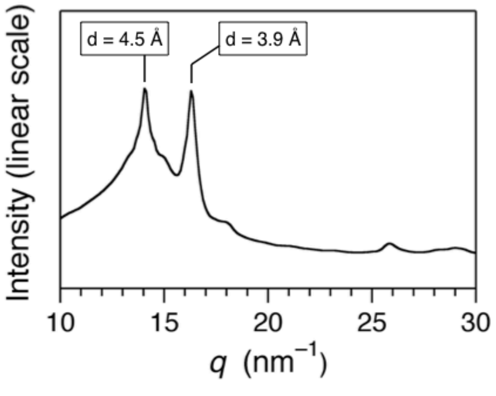

Figure 7. One-dimensional WAXS profile for H-shaped block copolymer L_2CL_2 [2_2–23–2_2] collected at ambient temperature.

Polymer crystallization follows one of two possible mechanisms. In homogeneous nucleation, polymer chains can spontaneously aggregate and align with one another to form a crystallite, thereby serving as a nucleation site from which further crystallization can propagate. In contrast, polymer crystallization may occur from heterogeneous nucleation sites derived from impurities (e.g., catalyst residue, dust). The former case is energetically unfavorable and requires substantial supercooling for crystal nucleation and growth to occur. The latter case is the most energetically favorable, and is the dominant mechanism by which bulk polymers crystallize, since the alternative would require unattainably pristine samples void of impurities.[73] However, block copolymers offer a scenario in which homogeneous nucleation may predominate, or alternatively in which multiple crystallization events can take place independently from heterogeneities with different nucleating energy barriers due to confinement of the semi-crystalline block. For example, if the spherical domains described above contain only a few hundred polymeric chains, the probability of an isolated domain experiencing no heterogeneities becomes statistically relevant. Naturally, a considerable portion of the isolated domains may be absent of impurities, and thereby nucleate and crystallize by the homogeneous mechanism. Crystallization exotherms can provide substantive support to this claim; T_c should occur at significantly lower temperature compared with bulk crystallization as a result of the necessary supercooling for homogeneous nucleation.[74] Multiple crystallization exotherms are sometimes observed as multiple mechanisms may be at play. For example, small domain sizes (e.g., 5–50 nm) may contain several different types of heterogeneities with considerably different energetic barriers to critically nucleate crystallization. However, crystallization in one isolated domain is prevented from propagating through a barrier such as a glassy domain in a microphase separated block copolymer. Likewise, if the semi-crystalline component of a block copolymer occupies a continuous matrix phase, then crystallites nucleated by even a relatively small number of heterogeneities will rapidly propagate throughout the entire material, and a single exotherm is expected in the DSC cooling thermogram. The phenomenon of multiple crystallization mechanisms occurring simultaneously and independently is termed fractionated crystallization,[75, 76] and regularly occurs in block copolymers with semi-crystalline components due to the distinctly small domains accessible as a result of microphase separation.

Thermograms from DSC analysis of block copolymers with different architectures and a range of compositions (f_C = 0.2–1.0) reveal distinctly different behaviors (Figure 8; Table S1).

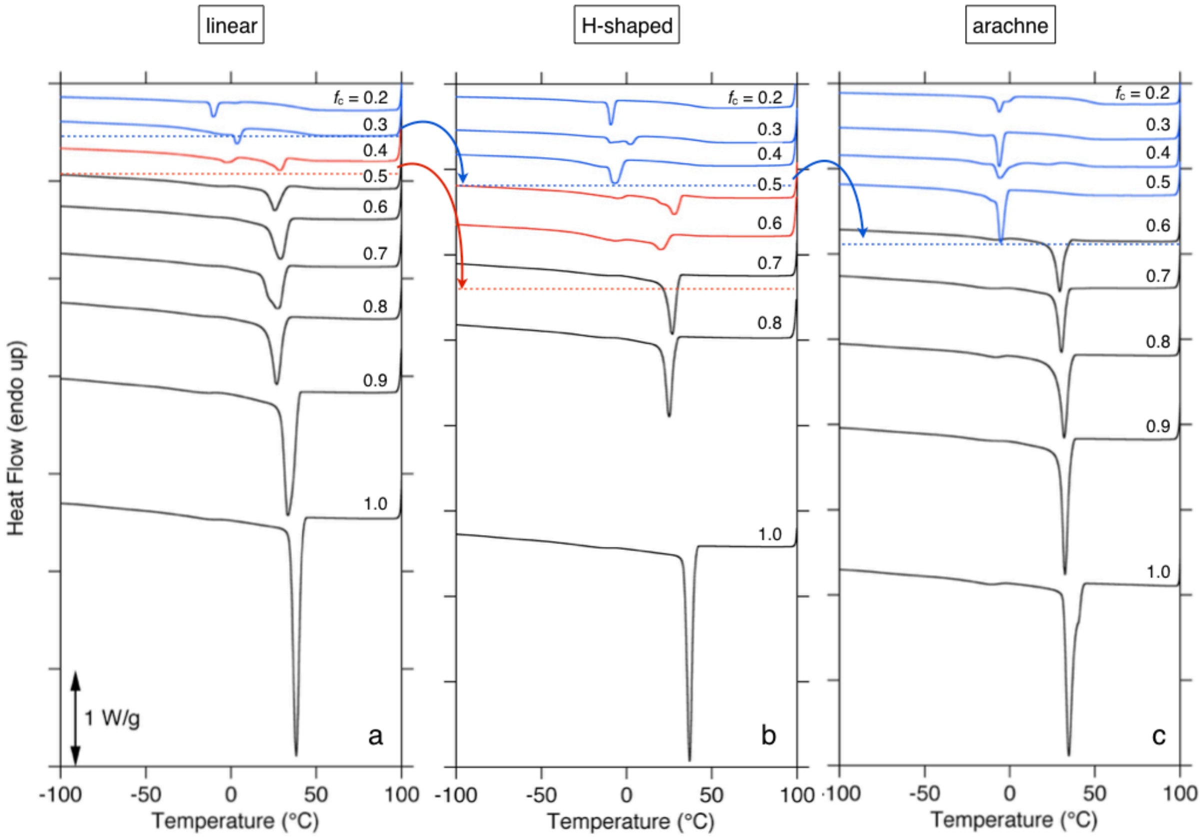

Figure 8. DSC cooling thermograms (rate = 10 °C min^{-1}) for block copolymers with a range of compositions with volume fractions of (approximate) PCOE (f_C) from 0.2–1.0 (provided as fractions above the corresponding thermograms) with (a) linear, (b) H-shaped[ii] and (c) arachnearm molecular architectures. Colors correspond to different regimes of crystallization behavior: only heterogeneous nucleation (black), mixed heterogeneous and homogeneous nucleation (red), and only homogeneous nucleation (blue).

[ii] There is no sample with H-shaped architecture and 90 vol. % PCOE

The nucleation and crystallization behavior depend on both composition and molecular architecture, which are intimately tied to the morphologies. The minimum in the exotherm occurs nearly identically at 36.5 °C ± 2 °C for the three PCOE homopolymers with different end-functionality number (i.e. HO_x–PCOE–OH_x with x = 1, 2, 4). The thermal behavior of PCOE homopolymers shown in Figure 8a–c are consistent with previous reports (Table S1).[58, 71] The T_m and T_c both are depressed in the triblock copolymers, in accordance with expectations for strongly segregated systems. The relative position of $T_{c,C}$ (≈ −10 to +34 °C) and $T_{g,L}$ (≈ +35 to +40 °C) suggests that crystallization typically occurs after vitrification during cooling, thus anchoring both ends of the PCOE segments during crystallization, and thereby retarding the chain diffusion that occurs during the chain packing associated with crystallization. These topological constraints manifest themselves as depressed T_m and T_c. Nonetheless, a single crystallization exotherm appears for the linear copolymers having f_C from 1.0–0.5 with $T_{c,C}$ ranging from 28–38 °C. Two distinct exotherms are observed with minima at 26 °C and –3 °C for the linear sample with f_C = 0.4. The sample with f_C equal to 0.3 exhibits a single sharp exotherm centered at +3 °C with a weak shoulder trailing toward lower temperature. The $T_{c,C}$ being approximately 35 °C lower than the PCOE homopolymer suggests an alternate nucleation mechanism as opposed to a mere artifact of anchored chain ends. Similarly, the sample with f_C equal to 0.2 shows a single exotherm positioned at –11 °C, again suggesting an alternate nucleation mechanism. The $T_{c,C}$ of this particular sample falls nearly 50 °C lower than the $T_{c,C}$ for the bulk PCOE material. The combined thermal results implicate a transition in the bulk morphology adopted in the melt. Specifically, a transition apparently occurs from the sample with f_C = 0.5, in which the PCOE occupies a continuous domain, to the sample with f_C = 0.4, in which a notable portion of the PCOE occupies isolated domains presumably containing fewer heterogeneities. The isolated domains correspondingly undergo nucleation at greater supercooling. This transition is consistent with the predicted position on the theoretical phase diagram from a lamellar to a cylindrical morphology, with the minority PCOE occupying isolated cylindrical domains. In actuality, the molecular characteristics prohibit the adoption of a well-ordered cylindrical morphology. Instead, the disordered morphological features suggested by the SAXS analysis likely cause a distribution of domain sizes, consistent with the mixed nucleation behavior attributed to the thermogram. Larger asymmetry results in increased curvature of the domain interfaces and therefore larger portions of the PCOE phase occupy isolated domains, accounting for the complete transition to homogeneous nucleation suggested by the thermograms for samples f_C = 0.3 and 0.2.

Similar transitions in nucleation behavior are observed for the H-shaped copolymers. However, the boundaries at which the transitions occur are shifted to higher volume fractions of PCOE due to the effects of topological contributions to the conformational asymmetry and thus the interfacial curvature. Complete heterogeneous nucleation and a corresponding single crystallization exotherm centered at $T_{c,C}$ = 27–37 °C are observed for samples with f_C ranging from 1.0 to 0.7, whereas mixed crystallization exotherms occur for samples with f_C equal to 0.6 and 0.5. Single crystallization exotherms with significantly depressed $T_{c,C}$ associated with homogeneous nucleation occur at –6, –11 and –8 °C in samples with f_C equal to 0.4, 0.3, and 0.2, respectively. Notably, the sample with f_C equal to 0.3 exhibits a multimodal crystallization exotherm with minima occurring at 2 °C and –11 °C, suggesting multiple nucleation mechanisms at work.

The boundary representing the transition to complete homogeneous nucleation occurs at a higher value of f_C for the arachnearm block copolymers than for the H-shaped copolymers (Figure 8c). There were no arachnearm samples that unambiguously exhibited coexisting nucleation mechanisms. That is, the sample with f_C = 0.6 shows a predominant crystallization exotherm occurring at $T_{c,C}$ = 30 °C, whereas the sample with f_C = 0.5 has a predominant exotherm with $T_{c,C}$ = –6 °C, a difference of 36 °C. Comparatively, the transition to predominantly homogeneous nucleation occurs between values of f_C = 0.5 and 0.6 for the arachnearm architecture, between f_C = 0.4 and 0.5 for the H-shaped architecture, and between f_C = 0.3 and 0.4 for the linear block copolymers. These results are consistent with the phase boundary shifts predicted by Milner for asymmetrically branched block copolymers.[15] The system accommodates the increasing energetic requirements for relaxing the PLA chains as the junction functionality increases by adjusting the curvature of the domain interfaces such that PLA occupies the convex side. The highly asymmetric arachnearm architecture, for example, presumably transitions to a spherical-like morphology at higher volume fractions than the less branched counterparts, which manifests itself as a transition to a homogeneous nucleation mechanism. This behavior is consistent with the DSC data associated with large supercoolings that result from the large proportion of small, isolated domains containing the semi-crystalline PCOE.

CONCLUSION

The bulk phase behavior has been described for several block copolymers with ABA linear architecture and A_2BA_2 H-shaped and A_4BA_4 arachnearm architectures at various compositions. Direct imaging of several samples revealed different morphologies adopted by the block copolymers as a function of branch functionality, with the curvature of the domain interfaces showing a strong dependence on both composition and molecular architecture. Specifically, a lamellar morphology was observed at highly asymmetric compositions ($f_L = 0.19$) for an H-shaped block copolymer. Likewise, two corresponding copolymers with linear and H-shaped architectures exhibited SAXS profiles characteristic of lamellar and cylindrical morphologies, respectively, with $f_L = 0.57$. Lastly, the crystallization behavior for a broad range of compositions was evaluated for linear, H-shaped, and arachnearm architectures, showing a strong dependence of nucleation mechanism on extent of branching. The crystallization behavior corroborates the observed phase behavior monitored by SAXS and TEM.

Collectively, we have demonstrated that architectural complexity can be utilized in PLA block copolymers to access morphologies that are inaccessible with conventional linear block copolymers. Importantly, the complexity was bestowed by using straightforward polymerization techniques; identical conditions were used to prepare the different architectures using conventional techniques with commercially available starting materials. Using this protocol, the mechanical and thermal properties of PLA block copolymers can be fine-tuned to the specific demands of various applications.

CONFLICTS OF INTEREST

There are no conflicts to declare.

ACKNOWLEDGMENTS

This work was funded by the National Science Foundation (DMR-0605880 and DMR-1006370 and DMR-1609459). L.M.P. acknowledges support from a fellowship awarded by the UMN Graduate School. B.M.C gratefully acknowledges the Office of the Dean at Luther College for financial support of a sabbatical leave of absence. Parts of this work were carried out at the University of Minnesota Characterization Facility, a member of the NSF-funded Materials Research Facilities Network (www.mrfn.org). Synchrotron SAXS analyses were conducted at the DuPont−Northwestern−Dow Collaborative Access Team (DND-CAT) located at Sector 5 of the Advanced Photon Source (APS), supported by E.I. DuPont de Nemours & Co., the Dow Chemical Company, and Northwestern University. Use of the APS, an Office of Science User Facility operated for the U.S. Department of Energy (DOE) Office of Science by Argonne National Laboratory, was supported by the U.S. DOE under Contract DE-AC02-06CH11357. We are grateful for careful reviewing of the manuscript by Nicholas Hampu and Claire Dingwell.

Electronic Supplementary Information (ESI) available: [details of any supplementary information available should be included here]. See DOI: 10.1039/x0xx00000x

REFERENCES

1. F. S. Bates, M. A. Hillmyer, T. P. Lodge, C. M. Bates, K. T. Delaney and G. H. Fredrickson, *Science*, 2012, **336**, 434-440.
2. N. Hadjichristidis, M. Pitsikalis and H. Iatrou, *Adv. Polym. Sci.*, 2005, **189**, 1-124.
3. H. Feng, X. Lu, W. Wang, N.-G. Kang and J. W. Mays, *Polymers*, 2017, **9**, 494.
4. Y. Deng, S. Zhang, G. Lu and X. Huang, *Polym. Chem.*, 2013, **4**, 1289-1299.
5. B. A. Temel, J. Amici, M. Sangermano and Y. Yagci, *J. Polym. Sci., Part A: Polym. Chem.*, 2013, **51**, 4601-4607.
6. X. Fan, Z. Wang, D. Yuan, Y. Sun, Z. Li and C. He, *Polym. Chem.*, 2014, **5**, 4069-4075.
7. B. V. K. J. Schmidt, M. Hetzer, H. Ritter and C. Barner-Kowollik, *Prog. Polym. Sci.*, 2014, **39**, 235-249.
8. F. Wurm and H. Frey, *Prog. Polym. Sci.*, 2011, **36**, 1-52.
9. M. Pitsikalis, S. Pispas, J. W. Mays and N. Hadjichristidis, *Adv. Polym. Sci.*, 1998, **135**, 1-137.
10. N. Hadjichristidis, M. Pitsikalis, S. Pispas and H. Iatrou, *Chem. Rev.*, 2001, **101**, 3747-3792.
11. N. Hadjichristidis, H. Iatrou, M. Pitsikalis and J. Mays, *Prog. Polym. Sci.*, 2006, **31**, 1068-1132.
12. A. Hirao, K. Murano, T. Oie, M. Uematsu, R. Goseki and Y. Matsuo, *Polym. Chem.*, 2011, **2**, 1219–1233.
13. L. M. Pitet, B. M. Chamberlain, A. W. Hauser and M. A. Hillmyer, *Macromolecules*, 2010, **43**, 8018-8025.
14. M. W. Matsen, *Macromolecules*, 2012, **45**, 2161-2165.
15. S. T. Milner, *Macromolecules*, 1994, **27**, 2333-2335.
16. C.-I. Huang and L.-F. Yang, *Macromolecules*, 2010, **43**, 9117-9125.
17. N. A. Lynd, F. T. Oyerokun, D. L. O‚ÄôDonoghue, D. L. Handlin and G. H. Fredrickson, *Macromolecules*, 2010, **43**, 3479-3486.
18. G. Floudas, N. Hadjichristidis, H. Iatrou, T. Pakula and E. W. Fischer, *Macromolecules*, 1994, **27**, 7735-7746.
19. G. Floudas, N. Hadjichristidis, H. Iatrou and T. Pakula, *Macromolecules*, 1996, **29**, 3139-3146.
20. N. Hadjichristidis, H. Iatrou, S. K. Behal, J. J. Chludzinski, M. M. Disko, R. T. Garner, K. S. Liang, D. J. Lohse and S. T. Milner, *Macromolecules*, 1993, **26**, 5812-5815.

21. D. J. Pochan, S. P. Gido, S. Pispas and J. W. Mays, *Macromolecules*, 1996, **29**, 5099-5105.

22. D. J. Pochan, S. P. Gido, S. Pispas, J. W. Mays, A. J. Ryan, J. P. A. Fairclough, I. W. Hamley and N. J. Terrill, *Macromolecules*, 1996, **29**, 5091-5098.

23. M. R. Whittaker, C. N. Urbani and M. J. Monteiro, *J. Am. Chem. Soc.*, 2006, **128**, 11360-11361.

24. C. Dyer, P. Driva, S. W. Sides, B. G. Sumpter, J. W. Mays, J. Chen, R. Kumar, M. Goswami and M. D. Dadmun, *Macromolecules*, 2013, **46**, 2023-2031.

25. T. Isono, I. Otsuka, Y. Kondo, S. Halila, S. Fort, C. Rochas, T. Satoh, R. Borsali and T. Kakuchi, *Macromolecules*, 2013, **46**, 1461-1469.

26. G. Floudas, N. Hadjichristidis, H. Iatrou, A. Avgeropoulos and T. Pakula, *Macromolecules*, 1998, **31**, 6943-6950.

27. Y.-G. Li, P.-J. Shi and C.-Y. Pan, *Macromolecules*, 2004, **37**, 5190-5195.

28. Y. Cong, B. Li, Y. Han, Y. Li and C. Pan, *Macromolecules*, 2005, **38**, 9836-9846.

29. J. Liu and C.-Y. Pan, *Polymer*, 2005, **46**, 11133-11141.

30. D.-H. Han and C.-Y. Pan, *J. Polym. Sci., Part A: Polym. Chem.*, 2006, **44**, 2794-2801.

31. A. Ekin and D. C. Webster, *Macromolecules*, 2006, **39**, 8659-8668.

32. T. Higashihara, R. Faust, K. Inoue and A. Hirao, *Macromolecules*, 2008, **41**, 5616-5625.

33. Y. H. Wei, B. Y. Li, Y. C. Han and C. Y. Pan, *Soft Matter*, 2008, **4**, 2507-2512.

34. C. Detrembleur, A. Debuigne, O. Altintas, M. Conradi, E. H. H. Wong, C. Jerome, C. Barner-Kowollik and T. Junkers, *Polym. Chem.*, 2012, **3**, 135-147.

35. P. A. Weimann, T. D. Jones, M. A. Hillmyer, F. S. Bates, J. D. Londono, Y. Melnichenko, G. D. Wignall and K. Almdal, *Macromolecules*, 1997, **30**, 3650-3657.

36. C. Lee, S. P. Gido, Y. Poulos, N. Hadjichristidis, N. B. Tan, S. F. Trevino and J. W. Mays, *J. Chem. Phys.*, 1997, **107**, 6460-6469.

37. M. W. Matsen and R. B. Thompson, *J. Chem. Phys.*, 1999, **111**, 7139–7146.

38. J. M. Widin, A. K. Schmitt, A. L. Schmitt, K. Im and M. K. Mahanthappa, *J. Am. Chem. Soc.*, 2012, **134**, 3834-3844.

39. A. K. Schmitt and M. K. Mahanthappa, *Macromolecules*, 2014, **47**, 4346-4356.

40. A. K. Schmitt and M. K. Mahanthappa, *Macromolecules*, 2017, **50**, 6779-6787.

41. Y. Wang and M. A. Hillmyer, *J. Polym. Sci., Part A: Polym. Chem.*, 2001, **39**, 2755-2766.

42. Y. Wang and M. A. Hillmyer, *Macromolecules*, 2000, **33**, 7395-7403.

43. N. A. Lynd and M. A. Hillmyer, *Macromolecules*, 2007, **40**, 8050–8055.
44. N. A. Lynd and M. A. Hillmyer, *Macromolecules*, 2005, **38**, 8803-8810.
45. K. S. Anderson, K. M. Schreck and M. A. Hillmyer, *Polym. Rev.*, 2008, **48**, 85-108.
46. K. S. Anderson, S. H. Lim and M. A. Hillmyer, *J. Appl. Polym. Sci.*, 2003, **89**, 3757-3768.
47. K. S. Anderson and M. A. Hillmyer, *Polymer*, 2004, **45**, 8809-8823.
48. E. W. Cochran, C. J. Garcia-Cervera and G. H. Fredrickson, *Macromolecules*, 2006, **39**, 2449-2451.
49. M. W. Matsen, *Eur. Phys. J. E: Soft Matter*, 2013, **36**, 1-7.
50. M. W. Matsen, *Eur. Phys. J. E: Soft Matter*, 2006, **21**, 199-207.
51. M. W. Matsen, *Phys. Rev. Lett.*, 2007, **99**, 148304/148301-148304/148304.
52. N. A. Lynd, A. J. Meuler and M. A. Hillmyer, *Prog. Polym. Sci.*, 2008, **33**, 875-893.
53. S. T. Milner, T. A. Witten and M. E. Cates, *Macromolecules*, 1989, **22**, 853-861.
54. M. Nadgorny, D. T. Gentekos, Z. Y. Xiao, S. P. Singleton, B. P. Fors and L. A. Connal, *Macromol. Rapid Commun.*, 2017, **38**, 1700352.
55. D. T. Gentekos and B. P. Fors, *Acs Macro Letters*, 2018, **7**, 677-682.
56. D. T. Gentekos, J. T. Jia, E. S. Tirado, K. P. Barteau, D. M. Smilgies, R. A. DiStasio and B. P. Fors, *J. Am. Chem. Soc.*, 2018, **140**, 4639-4648.
57. D. R. Witzke, J. J. Kolstad and R. Narayan, *Macromolecules*, 1997, **30**, 7075-7085.
58. W. A. Schneider and M. F. Müller, *J. Mol. Catal.*, 1988, **46**, 395–403.
59. J. M. Widin, M. Kim, A. K. Schmitt, E. Han, P. Gopalan and M. K. Mahanthappa, *Macromolecules*, 2013, **46**, 4472-4480.
60. M. E. Mackay, Y. Hong, M. Jeong, B. M. Tande, N. J. Wagner, S. Hong, S. P. Gido, R. Vestberg and C. J. Hawker, *Macromolecules*, 2002, **35**, 8391-8399.
61. C. Román, H. R. Fischer and E. W. Meijer, *Macromolecules*, 1999, **32**, 5525-5531.
62. H. Wang, W. Lu, W. Wang, P. N. Shah, K. Misichronis, N.-G. Kang and J. W. Mays, *Macromol. Chem. Phys.*, 2018, **219**, 1700254.
63. S. C. Schmidt and M. A. Hillmyer, *J. Polym. Sci., Part B: Polym. Phys.*, 2002, **40**, 2364-2376.
64. J. M. Widin, A. K. Schmitt, K. Im, A. L. Schmitt and M. K. Mahanthappa, *Macromolecules*, 2010, **43**, 7913-7915.
65. Y.-L. Loo, R. A. Register and A. J. Ryan, *Macromolecules*, 2002, **35**, 2365-2374.

66. M. W. Matsen and F. S. Bates, *J. Chem. Phys.*, 1997, **106**, 2436-2448.

67. Y.-L. Loo, R. A. Register, A. J. Ryan and G. T. Dee, *Macromolecules*, 2001, **34**, 8968-8977.

68. I. W. Hamley, *Adv. Polym. Sci.*, 1999, **148**, 114–137.

69. A. J. Muller, V. Balsamo and M. L. Arnal, *Adv. Polym. Sci.*, 2005, **190**, 1-63.

70. D. J. Quiram, R. A. Register and G. R. Marchand, *Macromolecules*, 1997, **30**, 4551-4558.

71. C. Liu, S. B. Chun, P. T. Mather, L. Zheng, E. H. Haley and E. B. Coughlin, *Macromolecules*, 2002, **35**, 9868-9874.

72. I. W. Bassi and G. Fagherazzi, *Eur. Polym. J.*, 1968, **4**, 123-132.

73. P. J. Barham, D. A. Jarvis and A. Keller, *J. Polym. Sci., Part B: Polym. Phys.*, 1982, **20**, 1733-1748.

74. O. O. Santana and A. J. Mueller, *Polym. Bull.*, 1994, **32**, 471-477.

75. H. Frensch, P. Harnischfeger and B. J. Jungnickel, *Acs Symposium Series*, 1989, **395**, 101-125.

76. H. Frensch and B. J. Jungnickel, *Colloid and Polymer Science*, 1989, **267**, 16-27.

TOC Graphic for:

Dispersity and Architecture Driven Bulk Phase Behavior and Confined Crystallization In Symmetric Branched Block Copolymers Containing Polylactide and Polycyclooctene

Louis M. Pitet, Bradley M. Chamberlain, Adam W. Hauser and Marc A. Hillmyer

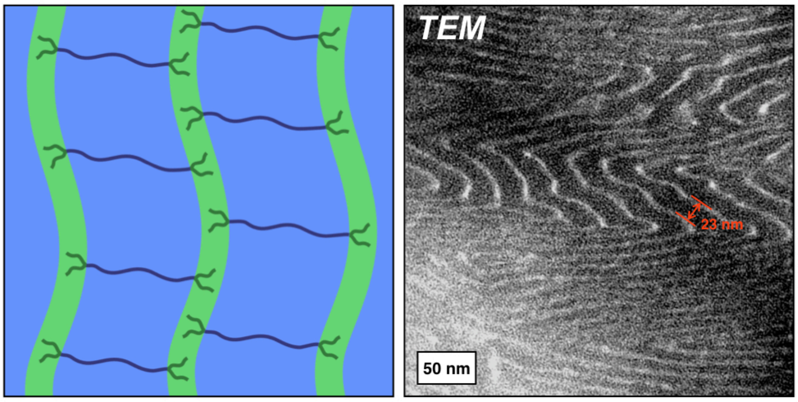

Highly asymmetric lamellae from disperse branched block copolymers